Journal of Solid State Chemistry **149,** 399–407 (2000)
doi:10.1006/jssc.1999.8565, available online at http://www.idealibrary.com on IDEAL®

Crystallite Size Effect on the Tetragonal-Monoclinic Transition of Undoped Nanocrystalline Zirconia Studied by XRD and Raman Spectrometry

E. Djurado,[1] P. Bouvier, and G. Lucazeau

Laboratoire d'Electrochimie et de Physico-Chimie des Matériaux et des Interfaces, Institut National Polytechnique de Grenoble, CNRS UMR 5631 associé à l'UJF, B.P. 75, 1130 rue de la Piscine, 38402 St. Martin d'Hères Cedex, France

Received August 4, 1999; in revised form October 21, 1999; accepted November 5, 1999

Two powdered batches of undoped zirconia, prepared by spray pyrolysis and characterized by 6.9 and 13.2 nm average crystallite size were annealed for different temperatures and for different times. The tetragonal–monoclinic phase transformation was monitored by Raman spectroscopy and X-ray diffraction. The evolution of parameters such as crystallite size, *c*/*a* unit cell parameter ratio, content of monoclinic and tetragonal zirconia, and Raman wavenumbers was found to differ from one batch to the other. The destabilization of the tetragonal phase appears for the 10 to 40 nm crystallite size range and as a sudden phenomenon. The critical size range varies with preparation. The wavenumber shifts were also discussed on the basis of internal stresses associated with mechanical balance between the surface and volume states. © 2000 Academic Press

Key Words: **undoped tetragonal nanocrystalline zirconia; monoclinic phase; crystallite size; Raman spectroscopy; XRD.**

1. INTRODUCTION

It is expected that nanostructured materials (i.e., grain size less than 100 nm) present different properties from those of more conventional materials with grain structures on a coarser scale. For instance, He *et al.* (1) have shown that fine-grained zirconia exhibits better wear resistance than the coarse-grained material. Tetragonal undoped zirconia which is a metastable phase at lower temperature than the well-known high-temperature zirconia in the 1170–2370°C temperature range (2, 3) could be stabilized by fine crystallites. Many controversies are reported in the literature about the factors affecting the nucleation of tetragonal zirconia transformation. Stabilization of tetragonal zirconia mainly depends on the amount of stabilizer (4, 5) and the stabilizer distribution (6), the precipitation pH values during the synthesis route (7), the grain size of the tetragonal powder (8–10), water vapor in crystallite growth (11, 7), and intrinsic defects such as vacancies in the anionic sublattice and strain within the grains (12–15). Moreover, the existence of a large stress gradient at the metal/oxide interface of zircaloy oxidation films used in nuclear industry is believed to stabilize the dense tetragonal form at the interface and to limit the corrosion rate (16). Among the main factors influencing the stability of tetragonal zirconia, S. Lawson reported that the purity of tetragonal powders is an inhibitor of its transformation and that impurities act as transformation nucleation points along grain boundaries because they cause strain and thermal stresses.

The purpose of this paper is to investigate the behavior of two powdered batches, initially characterized by 6.9 and 13.2 nm average crystallite sizes, versus thermal treatment. This present paper will not focus on the influence of water content and the role of protons in the destabilization of nanosized zirconia phases but on the crystallite size effect and on the c/a parameters ratio. The tetragonal-to-monoclinic transformation is studied using XRD and Raman spectroscopy and is aimed to model Zr oxidation. Indeed, Zr oxidation can involve the formation of nanophases located at the metal–oxide interface which are difficult to detect by X-ray diffraction, even under grazing incidence. Raman spectrometry has been selected because of its ability to identify amorphous phases (as, e.g., nanophases). A recent study of nanometric size effect on monoclinic zirconia was reported in the literature (17). Spectral changes reported in this latter study and considered as specific of nanometric character are quite small compared, for instance, to those recently observed on nanocrystallites of SnO_2 (18).

2. EXPERIMENTAL

2.1. Powder Preparation

Undoped zirconia powders were prepared by the spray-pyrolysis technique using an ultrasonic atomizer (19). The

[1] To whom correspondence should be addressed. Fax: 33 (0) 4 76 82 66 70. E-mail: Elisabeth.Djurado@lepmi.inpg.fr.

0022-4596/00 $35.00

TABLE 1
Spray-Pyrolysis Conditions and Resulting Crystallite Sizes Measured from X-Ray Line Broadening for Two Batches of ZrO_2 Powders

Batch No.	Concentration (mol L^{-1})	Frequency (kHz)	Flow rate (L min^{-1})	Temperature (°C)	Crystallite size (nm)
I	2.5×10^{-2}	1.7×10^3	6	600	6.9
II	2.5×10^{-2}	850	3	900	13.2

precursor solution consisted of zirconyl nitrate hydrate ($ZrO(NO_3)_2$, Aldrich) dissolved in distilled water at 2.5×10^{-2} mol L^{-1} concentration. The aqueous solution was atomized by a high-frequency ultrasonic mist generator. We used two piezoelectric ceramic transducers for which the frequencies were respectively 850 kHz or 1.7 MHz. The carrier gas ($N_2 + O_2$ mixture) carried the aerosol with flow rates of 3 or 6 L min^{-1} through a tubular furnace, heated at either 600 or 900°C after a very short pyrolysis time (typically, 8 s for a 6 L min^{-1} flow rate). Table 1 summarizes the experimental conditions for the synthesis of two powder batches. At the difference with other methods of "chimie douce" (20), the present synthesis route led to nanocrystalline powders of pure zirconia in which no amorphous phase was detected, neither with X-ray diffraction nor with Raman spectrometry. It was not the case with the spray-pyrolysis route performed at 450°C and starting from metal–organic precursors (21). The presently prepared compounds are referred to as I-6.9 and II-13.2, where I and II represent the batch and 6.9 and 13.2 represent the average crystallite size (in nm) which was estimated from X-ray line broadening measurements.

In a second step, each powder batch, respectively I-6.9 and II-13.2, was then heated in air, in a platinum crucible for various thermal treatments (in the 600–1400°C temperature range with heating and cooling rates of 5°C/min and in the 15 min to 2 h time range) to increase the crystallite size. Two different sets of samples were obtained (Table 2). The reproducibility of the crystallite size for a given thermal treatment was checked.

2.2. Powder Characterization

Particle size, morphology of powders, and crystallite size were examined using transmission electron microscopy (JEOL 300CX).

Powder X-ray diffraction was carried out using a Siemens D500 $\theta/2\theta$ diffractometer with the Bragg Brentano geometry from 20° to 80° in 2θ (0.03° in 2θ step, 12 s as a counting time) equipped with a rear monochromator ($CuK\alpha_1$ radiation, $\lambda = 1.5406$ Å). High-purity silicon was used as the standard for all scans to precisely measure the zero shift and the instrumental resolution. Positions and FWHM of XRD peaks were determined by a decomposition into pseudo-Voigt-shaped peaks with ABFit software (ILL, Grenoble, France). The crystallite size was calculated using the Debye–Scherrer formula for the *111* and *222* peaks of the tetragonal phase (22): $D = 0.9\lambda/\beta \cos\theta$, where D is the crystallite size (in nm), λ the wavelength (in nm), β the corrected FWHM from high-purity silicon (in radian), and θ the diffraction angle. Cell parameter refinements were performed using the software CELREF (by Laugier and Filhol, ILL, Grenoble, France).

Room-temperature Raman spectra were recorded using a DILOR XY multichannel spectrometer equipped with a CCD detector refrigerated by liquid nitrogen. The 514.53 nm (green) and the 488 nm (blue) excitation lines of an argon ion laser were used. All experiments were carried out using a laser power of 20 mW in macroscopic back-scattering geometry. Low-temperature micro-Raman was carried down to the liquid nitrogen temperature (−175°C). Position and half width at half maximum (HWHM) of Raman bands were obtained by decomposition into Lorentzian-shaped peaks with PeakFit software (v. 4.0, Jandel Scientific).

Initial water content of the as-prepared I-6.9 and II-13.2 was obtained from thermal gravimetric analysis (TGA) and was found to be about 5 and 1 wt%, respectively. This was confirmed by IR measurements from relative absorption at about 3250 to that at 580 cm^{-1}. We should notice that the

TABLE 2
Referred Samples for Two Batches of Zirconia Powders

Annealing conditions in air	Batch I, I-6.9	Batch II, II-13.2
No annealing	6.9	13.2
600°C, 15 min	8.3	13.8
600°C, 2 h	8.9	13.3
800°C, 2 h	20.3	18.0
900°C, 15 min	21.0	21.8
950°C, 1 h	30.1	22.0
1000°C, 1 h	36.3	25.5
1400°C, 2 h	65.2	85.8

subsequent thermal treatments of these samples are of course accompanied by a departure of water and this process is under study (23).

3. RESULTS

3.1. TEM on I-6.9, II-13.2, and I-20.3 Powders

Microscopic examinations of the as-prepared powders show submicron spherical particles consisting of aggregated nanocrystallites. Figure 1 shows bright-field TEM micrographs of as-prepared I-6.9 and II-13.2 powders (a and b) as well as I-20.3 powder resulting from 800°C/2 h thermal treatment (c). II-13.2 powder exhibits a homogeneous repartition of crystallite size inside each agglomerate and the size is close to that extracted from X-ray line broadening. This is not clearly the case for I-6.9 powder and it is much more difficult to conclude the monodisperse aspect of the size distribution.

3.2. XRD Characterization

Figure 2a shows zoomed XRD patterns (20°–45° in 2θ) of I-6.9 versus thermal treatment. The crystallite size increases from 6.9 to 65.2 nm (see Table 2). The as-prepared I-6.9 diffractogram was identified with tetragonal zirconia crystallizing in the $P4_2/nmc$ space group which was obtained at 1250°C. An average crystallite size of 6.9 nm was deduced from the broadening of the *111* line (FWHM = 1.11° compared to the *111* line of high-purity silicon FWHM = 0.15°). At $2\theta = 35°$ the absence of splitting into *200* and *002* diffraction lines, characteristic of the tetragonal structure, may be attributed either to the broadening of diffraction lines due to a small crystallite size or to the deviance from the tetragonality toward a less anisotropic structure ($c/a \approx 1$). Cell parameter refinement for I-6.9 leads to $a = 0.5092 \pm 9 \times 10^{-4}$ nm and $c = 0.5165 \pm 8 \times 10^{-4}$ nm ($c/a = 1.014$). At this stage, one can assert that the broadening of XRD lines is mainly due to the nanoscale size of crystallites and not to the deviance from tetragonality. The simultaneous presence of tetragonal and monoclinic ZrO_2 was clearly detected with increasing crystallite size. A continuous c/a ratio increase is presented in Fig. 3 for an increase of crystallite sizes. It is interesting to note that structural characteristics of this tetragonal phase are close to those of other zirconia of similar crystallite sizes and prepared via a hydrolysis route from chlorides (20). For a larger crystallite size (65.2 nm), monoclinic ZrO_2 appears (Fig. 2a), (24). Cell parameter refinement leads to $a = 0.53144 \pm 5 \times 10^{-5}$ nm, $b = 0.52100 \pm 4 \times 10^{-5}$ nm, $c = 0.51476 \pm 5 \times 10^{-5}$ nm, and $\beta = 99.218 \pm 0.009$. Figure 2b shows zoomed XRD patterns (20°–45° in 2θ) of II-13.2 versus thermal treatment. The crystallite size increases from 13.2 to 85.8 nm (see Table 2). The pure tetragonal crystalline phase was characterized by an average ≈ 13 nm crystallite size. Monoclinic lines clearly appeared for an ≈ 22 nm crystallite size, giving rise to a pure monoclinic phase. A striking change of c/a values for II-13.2 was observed in a smaller crystallite size domain, ≈ 22 nm (Fig. 3), with the simultaneous appearance of monoclinic ZrO_2, c/a ratio reaching a plateau for

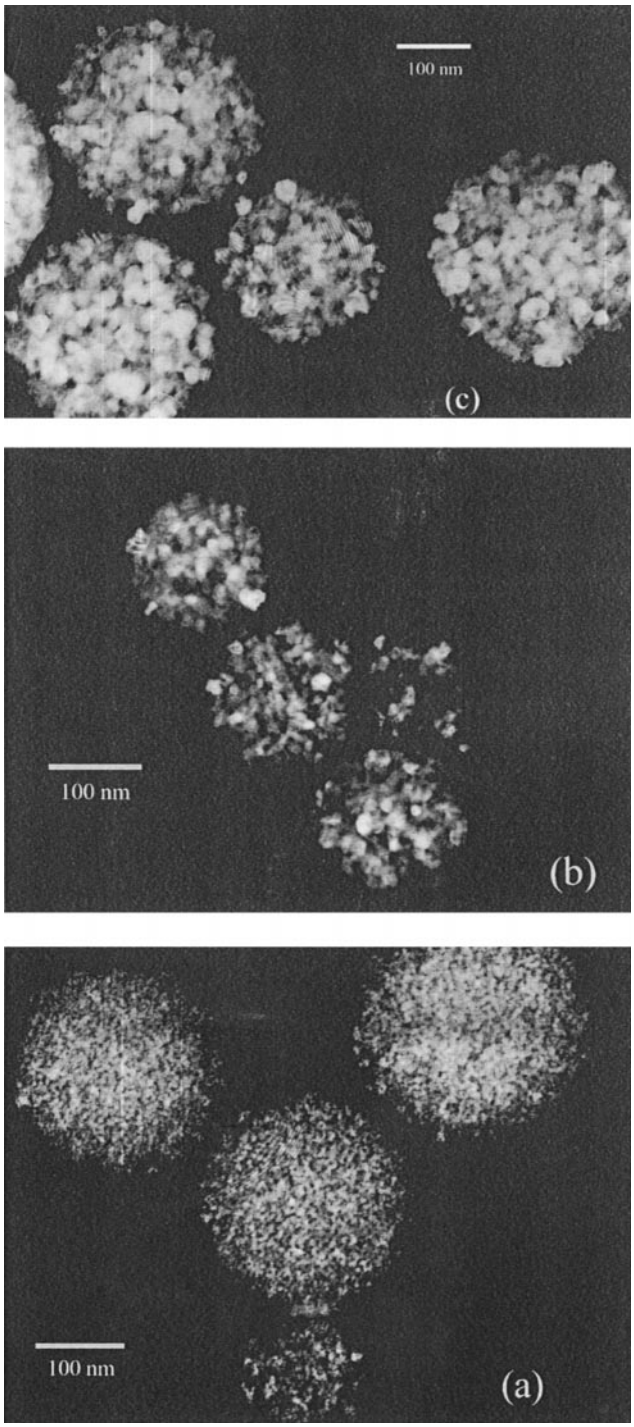

FIG. 1. Bright-field TEM micrographs of I-6.9, II-13.2, and I-20 powders (1 cm indicates 0.1 μm).

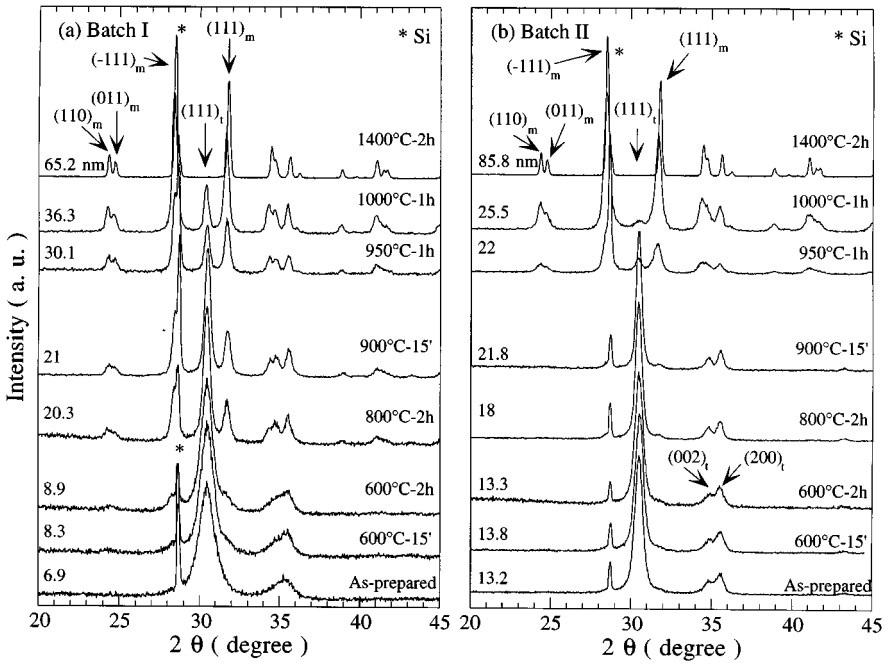

FIG. 2. X-ray diffractograms of (a) I-6.9 and (b) II-13.2 versus crystallite size increase. Monoclinic and tetragonal ZrO_2 are indexed according to #37-1484 and #42-1164 JCPDS cards, respectively.

both batches and for the 25 nm crystallite size. An $\approx 5\%$ relative variation of the unit cell volume is observed during phase transformation in agreement with the literature data (25).

3.3. Raman Spectroscopy

The continuous transformation of the tetragonal-to-monoclinic phase was also observed with Raman spectroscopy. Figure 4a shows Raman spectra of I-6.9 powder versus crystallite size. For a small crystallite size, except for the presence of two weak bands at 179 and 189 cm^{-1} belonging to a small proportion of monoclinic ZrO_2, one observes the six Raman active modes of the tetragonal form (D_{4h}^{15}). For a large crystallite size (65.2 nm) the structure is purely monoclinic (C_{2h}^{5}); it can be confirmed by the observation of 16 Raman modes from the 18 ($9A_{1g} + 9B_{1g}$) expected by symmetry analysis (26). As the crystallite size increased from 8.3 to 36.3 nm, tetragonal bands around 600, 480, and 320 cm^{-1} are progressively replaced by monoclinic bands at 630–618, 476, and 347–335–306 cm^{-1}, respectively.

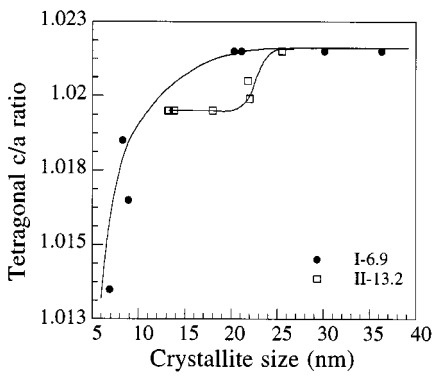

FIG. 3. c/a ratio measured by X-ray refinements versus crystallite size increase.

Figure 4b represents Raman spectra of II-13.2 powder versus thermal treatment. Here, the transformation is observed in a much narrower range of crystallite sizes comprised between 21.8 and 25.5 nm.

Raman frequency variation versus crystallite size of noninterfering modes belonging to tetragonal and monoclinic forms are presented in Fig. 5. The critical size R_c above which tetragonal zirconia disappears is equal to 23 nm in the II-13.2 batch and is much more difficult to define in batch I. For the I-6.9 batch, the 150 and 270 cm^{-1} tetragonal modes strongly decrease when the crystallite size increases (Figs. 5a and 5d, respectively) while on the contrary, no substantial frequency variation is detected for the II-13.2 batch below R_c. If we focus on the monoclinic phase below R_c, we observe a positive or constant variation of 178 and 189 cm^{-1} modes when the crystallite size increases (Figs. 5c and 5d) contrary to the tetragonal phase. The small proportion of the monoclinic phase in the II-13.2 batch generates large error bars on the wavenumber

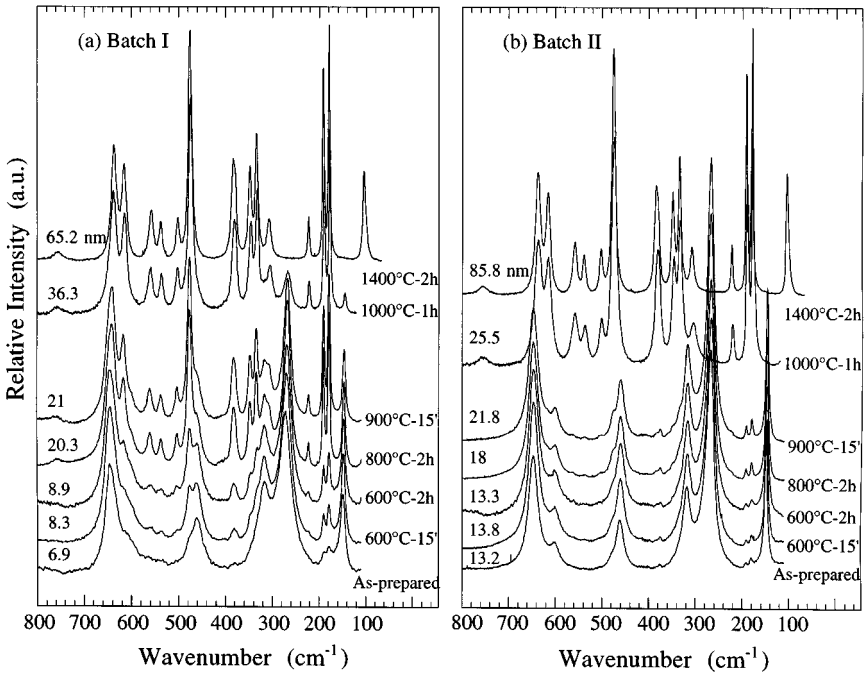

FIG. 4. Raman spectra of (a) I-6.9 and (b) II-13.2 powder versus crystallite size increase.

measurement. When the crystallite size increases, a discontinuity is observed at R_c and above R_c the monoclinic wavenumbers increase to reach the bulk frequency.

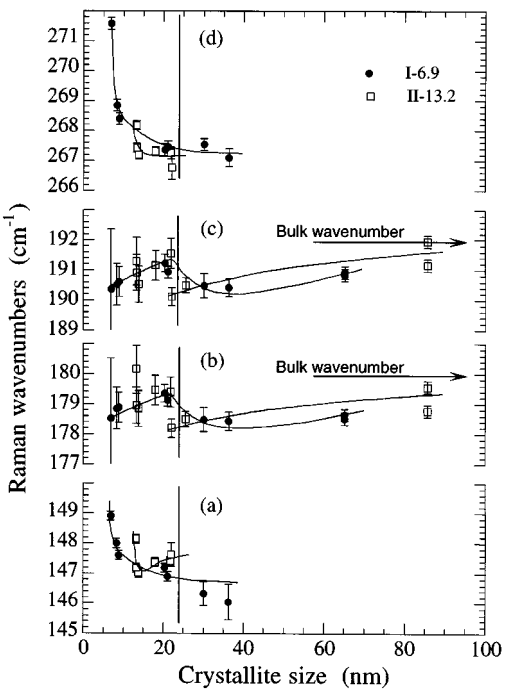

FIG. 5. Wavenumbers versus crystallite sizes of tetragonal Raman bands at (a) 150 and (d) 260 cm^{-1} and monoclinic Raman bands at (b) 180 and (c) 190 cm^{-1} of I-6.9 and II-13.2 batches. A vertical line is reported for the critical size R_c above which tetragonal zirconia disappears.

The HWHM of Raman modes at 150 and 260 cm^{-1} for the two different batches are depicted versus the crystallite size in Fig. 6. A continuous decrease of HWHM for all the modes was observed with crystallite size expansion.

Typical Raman spectra of II-18 powder at room temperature (25°C) and liquid nitrogen temperature (−175°C) are presented in Fig. 7. The decreasing temperature triggered off a spectacular narrowing of all Raman bands and a positive frequency shift without simultaneous destabilization of the

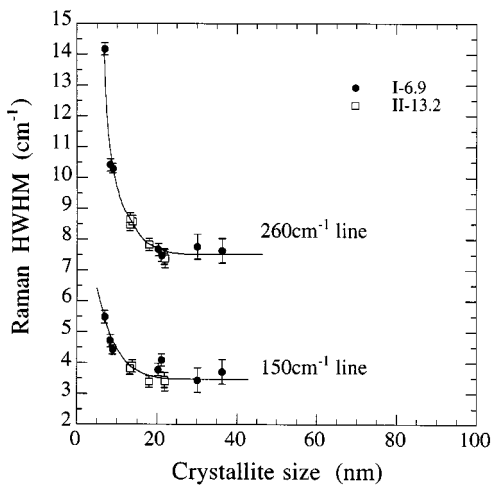

FIG. 6. hwhm versus crystallite sizes of Raman bands at 150 and 260 cm^{-1} for I-6.9 and II-13.2 batches.

tetragonal structure. This thermal narrowing effect is stronger for low-frequency modes.

3.4. Comparative Quantitative XRD and Raman Analysis

Quantitative XRD and Raman analysis of the tetragonal/monoclinic two-phase zirconia were already reported by several authors (27–31). Calibration curves for mixtures of monoclinic and tetragonal powders were respectively constructed by Evans *et al.* from X-ray diffraction results (28) and Kim *et al.* from Raman data (29). The monoclinic content, referred to as f_m, was obtained (i) from XRD patterns using the following equation,

$$f_m = I_m(111)/\{I_t(111) + I_m(111)\},$$

or (ii) from Raman spectra using the following equation (30),

$$f_m = \sqrt{0.19 - \frac{0.13}{X_m - 1.01}} - 0.56,$$

with $X_m = \{I_m(180\ \mathrm{cm}^{-1}) + I_m(192\ \mathrm{cm}^{-1})\}/\{I_m(180\ \mathrm{cm}^{-1}) + I_m(192\ \mathrm{cm}^{-1}) + I_t(148\ \mathrm{cm}^{-1})\}$.

The monoclinic ZrO_2 content versus crystallite size is presented in Fig. 8 from XRD and Raman data. The global behavior is similar for the two techniques. For II-13.2 powder batch, a drop from t-ZrO_2 to m-ZrO_2 for a crystallite size >21 nm was observed while a continuous phase transformation was detected for I-6.9. Moreover, as it was first stated by Kim *et al.* (29), we should notice that Raman spectroscopy is much more appropriated to detect traces of the monoclinic phase (see zoom in Fig. 8).

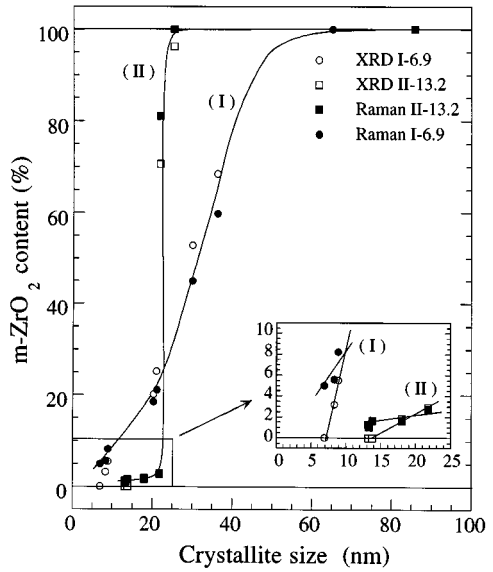

FIG. 8. Monoclinic content versus crystallite size determined respectively by X-ray diffraction and Raman spectroscopy for I-6.9 and II-13.2 batches. A zoom of low monoclinic content versus low crystallite range is also given.

4. DISCUSSION

Crystallite sizes determined by XRD and TEM are found to be of the same order of magnitude. Dark field TEM micrographs (Fig. 1) showed the true geometric size of crystallites, i.e., the true physical value, whereas crystallite diameters calculated from peak broadening of XRD patterns are the measurements of a mean sphere diameter. Moreover, the crystallite size of tetragonal and monoclinic forms which appear after annealing are found to be quite similar.

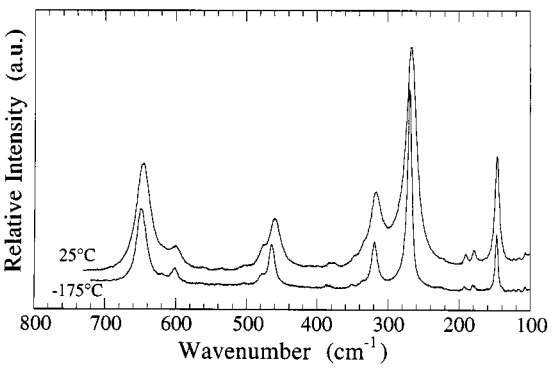

FIG. 7. Raman spectra of II-18 at decreasing temperatures from 25°C to −175°C.

According to XRD and Raman data, the increase of crystallite size with annealing treatments of undoped ZrO_2 induces a tetragonal-to-monoclinic phase transformation (see Fig. 8). These results are in good agreement with those reported by Gupta *et al.* (10). Stefanic *et al.* (7) reported that the destabilization of undoped zirconia by thermal treatment is believed to be due to dehydroxylization for annealing above 400°C. In the present study, the destabilization rate differs from one batch to the other. For I-6.9 powder which presents the smallest crystallite size, the highest content of the monoclinic phase (5 wt%) and of water (5 wt%), the structural transformation is continuous with a coexistence of the monoclinic and tetragonal phases in a broad domain of crystallite sizes extending up to 45 nm. However, for II-13.2 which is characterized by larger crystallites, 1 wt% of the monoclinic phase and 1 wt% of water, the transformation appears more critical and the tetragonal phase suddenly disappears above ≈ 23 nm. This latter critical phenomenon can be well explained by Garvie *et al.*'s theory (32). The authors assumed that an excess of surface energy in smaller crystallites should stabilize the pure tetragonal phase. Here, the critical size is $R_c = 23$ nm, whereas

Garvie *et al.* estimated it to be around 30 nm (32). Below R_c, the departure of water due to thermal treatments does not influence the tetragonal stability. The thermal behavior of I-6.9 cannot be adequatly understood by the surface energy theory reported by Garvie *et al.* Here, the size dispersion and the global content of water and of the monoclinic phase of the powders must play a major role in these two different behaviors. Mitsuhashi *et al.* (12) showed from mechanical treatment that a tetragonal and monoclinic mixture are much more difficult to transform into a monoclinic than a single tetragonal domain. The authors suggested that the domain boundaries may suppress the t → m transformation. Note that water could be located in these boundaries. Stefanic *et al.* (7) assumed that the rate of the t → m transformation decreases with an increase of m-ZrO_2 content. Let us compare the influence of thermal treatment on phase fractions of nanocrystalline zirconia prepared by different routes. A recent study carried out by Benfer *et al.* (33) focused on zirconia prepared by (i) CVD from organic precursors and (ii) flame hydrolysis from $ZrCl_4$ (Degussa). Our zirconia were prepared by pyrolysis of nitrates at 600°C (I-6.9) and 900°C (II-13.2). In all cases, a much higher tetragonal phase fraction is associated with larger crystallite sizes. However, it is clear that differences in the monoclinic appearance rate with temperature occur depending on the synthesis conditions (i.e., raw products, temperature, atmosphere, etc.). Our new experimental data provide a valid comparison of two batches which were prepared by the same procedure, playing with only the properly controlled temperature parameter. The different annealings were also carried out in the same furnace.

The examination of c/a ratios is directly correlated with relative tetragonal proportion for increasing crystallite sizes. For II-13.2 critical behavior is once again observed (Fig. 3). At higher sizes, c/a reaches a plateau at $c/a = 1.022$ which is very close to the 1.025 reported for undoped zirconia from the XRD pattern taken at 1250°C. The larger c/a ratio (1.022) found for larger crystallites should lead to larger anisotropic stress relaxation.

Let us compare the Raman study of our zirconia with a recent work (17) for similar sizes. Contrary to Ref. (17), zirconia nanocrystallites do not present any surface modes, the crystallites likely being too large for allowing a sufficient proportion of surface atoms. For instance, for a 7 nm spherical particle, there are only 4% of surface atoms. These authors mentioned the presence of a strong band close to 1030 cm^{-1} which they assigned to a surface second order mode. We also observe the presence of intense peaks between 1000 and 1400 cm^{-1} (Fig. 9) which can be unambiguously attributed to fluorescence peaks due to presumably defects resulting from the initial preparation. Notice that this fluorescence is the sum of two different fluorescence patterns (34). The larger one is related to tetragonal zirconia while the weaker one belongs to the monoclinic phase which is a minority in the sample. The patterns are different because the cationic coordination number changes from 8 to 7 with the structural transition from tetragonal to monoclinic. This fluorescence deserves to be more precisely analyzed in the future.

The bulk frequencies exhibit some substantial variation with increasing size. The size dependence of wavenumbers can be discussed in terms of a phonon confinement model (35) and also in terms of internal stresses which can result

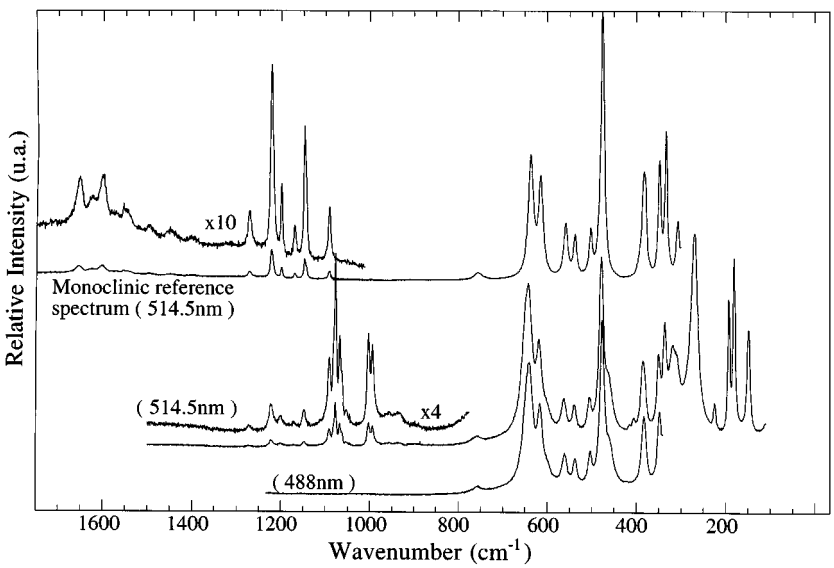

FIG. 9. Raman spectra of I-20.3 powder recorded with the 514.5 nm (green) and 488.8 nm (blue) excitation line of an argon ion laser.

from the defects linked to the large specific area of the crystallites. For I-6.9, the wavenumbers of volume modes of tetragonal zirconia observed at 148 and 270 cm^{-1} decrease with increasing crystallite size. These trends are not so clearly evidenced for II-13.2. Considering the grüneisen mode constants obtained in a recent high pressure study of nanometric tetragonal zirconia (36) ($\gamma_{148} = +1.75\ cm^{-1}$/GPa, $\gamma_{270} = -3.59\ cm^{-1}$/GPa), the same red shift of the 148 and 270 cm^{-1} modes cannot be explained by an isostatic stress variation when the crystallite size increases. Actually, this could be due to the fact that the internal pressure is anisotropic as it can be deduced from the increase of the *c* parameter with the crystallite size while the *a* parameter is nearly invariant. Thus, it is difficult to conclude on the sign of the stresses. Assuming that vacancies are preferably located in the near surface region and that the accomodation of oxygen at the surface activates the transition, one can predict that the transformation induces a volume expansion in the near surface layer and thus a compression in the core of the crystallite. As in Ref. (17), the wavenumbers of monoclinic crystallites exhibit a discontinuity at R_c and then those above R_c exhibit a slight increase and tend toward those measured in a bulk sample (relaxed monoclinic zirconia). This discontinuity could correspond to anisotropic stress relaxation which is difficult to quantify. Moreover, from general considerations such as the anisotropic stress gradient in each crystallite, the size distribution inside the particule, presence of defects, or finally phonon confinement, one can expect a general broadening of Raman bands for small crystallite sizes. The Raman lines of II-18 powder surprisingly become quite narrow (at the difference of 3 mol% Y^{3+} stabilized zirconia) with decreasing temperature. This observation is a clear proof that both the confinement model and stress distribution cannot explain the HWHM of Raman bands at room temperature. Consequently, this remarkable behavior in nanometric crystallites is typical of crystallites without defects presenting harmonic behavior with similar Raman HWHM. Moreover, the small HWHM confirms the homogeneity of crystallite sizes. On the contrary, the Raman HWHM of I-6.9 are rather broad and we observe a substantial decrease with thermal treatment. No such important narrowing of Raman bands was observed at low temperature (37). Here, the relative influence of intrinsic defects, confinement effects, and size distribution cannot be easily decorrelated.

To evidence the nature, the quantity, and the distribution of defects in the crystallites such as dislocations, surstructures, microdomains, TEM, and low-temperature Raman spectrometry are in progress.

5. CONCLUSION

This present work is focused on X-ray diffraction and Raman spectrometry characterizations of undoped nanocrystalline tetragonal zirconia and their transformation into monoclinic phase versus thermal treatments. The rate of transformation is found quite similar by both techniques. A slightly higher Raman sensitivity is found for the detection of low monoclinic content.

The crystallite size effect on Raman spectra remains modest as long as the surface contribution is smaller than the volume contribution. Tetragonal Raman wavenumber shifts are negative and lower than 4 cm^{-1} in the 6 to 15 nm crystallite size range. The tetragonal HWHM is reduced by a factor of 2 in this crystallite size range. These results did not favour the confinement model nor a mechanical stress model.

The critical crystallite size for the transformation is well defined (23 nm) for the sample which contains only 1 wt% monoclinic zirconia and 1 wt% water in its initial state (powder prepared at higher temperature and lower speed). This observation is in good agreement with Garvie's thermodynamic model. Reciprocally, for the compound initially rich in monoclinic phase (5 wt%) and in water (5 wt%), the transformation is delayed.

Contrary to the literature about monoclinic nanometric powders (17), Raman modes have not been observed around 1000 cm^{-1}. On the other hand, monoclinic and tetragonal phases present different fluorescence bands in this frequency range.

ACKNOWLEDGMENTS

The authors would like to thank N. Rosman for his technical assistance for Raman measurements.

REFERENCES

1. Y. J. He, A. J. A. Winnubst, A. J. Burggraaf, H. Verweij, P. G. van der Varst, and B. G. De With, *J. Am. Ceram. Soc.* **79,** 3090 (1996).
2. H. J. Scott, *J. Mater. Sci.* **10,** 1527 (1975).
3. G. Teufer, *Acta Crystallogr.* **15,** 1187 (1962).
4. K. Haberko and R. Pampuch, *Ceram. Int.* **9,** 8 (1983).
5. K. Tsukuma, Y. Kubota, and T. Tsukidate, "Advances in Ceramics, Science and Technology of Zirconia II" (N. Claussen, M. Ruehle, and A. H. Heuer, Eds.), Vol. 12, p. 382. The American Ceramic Society Inc., Columbus, OH, 1984.
6. S. Lawson, *J. Eur. Ceram. Soc.* **15,** 485 (1995).
7. G. Stefanic, S. Music, B. Grzeta, S. Popovic, and A. Sekulic, *J. Phys. Chem. Solids* **59,** 879 (1998).
8. R. C. Garvie, R. H. Hannink, and R. T. Pascoe, *Nature* (*London*) **258,** 703 (1975).
9. F. F. Lange, *J. Mater. Sci.* **17,** 225 (1982).
10. T. K. Gupta, J. H. Bechtold, R. C. Kuznicki, L. H. Cadoff, and B. R. Rossing, *J. Mater. Sci.* **12,** 2421 (1977).
11. Y. Murase and E. Kato, *J. Am. Ceram. Soc.* **66,** 196 (1982).
12. T. Mitsuhashi, M. Ichihara, and U. Tatsuke, *J. Am. Ceram. Soc.* **57,** 97 (1974).
13. A. P. Mirgorodsky, M. B. Smirnov, and P. E. Quintard, *Phys. Rev. B* **55,** 19 (1997).
14. A. H. Heuer, M. Ruhle, and D. B. Marshall, *J. Am. Ceram. Soc.* **73,** 1084 (1990).

15. K. Negita and H. Takao, *J. Phys. Chem. Solids* **50,** 325 (1989).
16. J. Godlewski, P. Bouvier, G. Lucazeau, and L. Fayette, "12th International Symposium 'Zirconium in Nuclear Industry,'" Toronto, 1998, AST-STP 1343, G. D. Moan and G. P. Sabol, Eds., American Society for testing and material, 1999.
17. G. G. Siu, M. J. Stokes, and Y. Liu, *Phys. Rev. B* **59,** 4 (1999).
18. L. Abello, B. Bochu, A. Gaskov, S. Koudryavtseva, G. Lucazeau, and M. Roumyantseva, *J. Solid State Chem.* **135,** 78 (1998).
19. E. Djurado and E. Meunier, *J. Solid State Chem.* **141,** 191 (1998).
20. X. Bokhimi, A. Morales, A. Garcia-Ruiz, T. D. Xiao, H. Chen, and P. R. Strutt, *J. Solid State Chem.* **142,** 409 (1999).
21. P. Murugavel, M. Kalaiselvam, A. R. Raju, and C. N. R. Rao, *J. Mater. Chem.* **7**(8), 1433 (1997).
22. A. Guinier, "Théorie et Technique de la radiocristallographie" (Dunod, Ed.), 3rd ed., Chap. 12, p. 482. Paris, 1964.
23. E. Djurado, C. Roux, and L. Dessemond, "12th International Conference on Solid State Ionics," Thessaloniki, 1999, June 6–12, 1999.
24. D. K. Smith and H. W. Newkirk, *Acta Crystallogr.* **18,** 983 (1965).
25. R. A. Cutler, J. R. Reynolds, and A. Jones, *J. Am. Ceram. Soc.* **75,** 2173 (1992).
26. D. Michel, M. Perez, Y. Jorba, and R. Collongues, *J. Raman Spectrosc.* **5,** 163 (1976).
27. E. D. Whitney, *Trans. Faraday Soc.* **61,** 1191 (1965).
28. P. A. Evans, R. Stevens, and J. G. P. Binner, *Br. Ceram. Trans. J.* **83,** 39 (1984).
29. B. K. Kim, J. W. Hahn, and K. R. Han, *J. Mater. Sci. Lett.* **16,** 669 (1997).
30. B. Alzyab, C. H. Perry, and R. P. Ingel, *J. Am. Ceram. Soc.* **70,** 760 (1987).
31. C. G. Kontoyannis and M. Orkoula, *J. Mater. Sci. Lett.* **29,** 5316 (1994).
32. R. C. Garvie, *J. Phys. Chem.* **69,** 1238 (1965).
33. S. Benfer and E. Knözinger, *J. Mater. Chem.* **9,** 1203 (1999).
34. I. M. Asher, B. Papanicolaou, and E. Anastassakis, *J. Phys. Chem. Solids* **37,** 221 (1976).
35. H. Richter, Z. P. Wang, and L. Ley, *Solid State Commun.* **39,** 625 (1981).
36. P. Bouvier and G. Lucazeau, *J. Phys. Chem. Solid*, 1999, in press.
37. P. Bouvier, E. Djurado, C. Ritter, and G. Lucazeau, to be published.